*Sensors & Transducers, Vol. 209, Issue 2, February 2017, pp. 35-44*

www.sensorsportal.com

**Sensors & Transducers**

Published by IFSA Publishing, S. L., 2017
http://www.sensorsportal.com

# Performance and Analysis of an Asynchronous Motor Drive with a New Modified Type-2 Neuro Fuzzy Based MPPT Controller Under Variable Irradiance and Variable Temperature

**Pakkiraiah B. and Durga Sukumar G.**
Department of Electrical and Electronics Engineering,
Vignan's Foundation for Science Technology and Research University,
Guntur, A.P, India-522213
E-mail: pakki1988@gmail.com, durgasukumar@gmail.com

*Received: 9 December 2016 /Accepted: 30 January 2017 /Published: 28 February 2017*

**Abstract:** In the present research, we have developed a new modified Type 2 neuro fuzzy (T2NF) based MPPT controller, which combines the advantages of fractional open circuit voltage (FCV), variable step and optimized P&O algorithm. It leads to a faster and better tracking and lower oscillations around the MPP to contribute higher efficiency. The simulation result shows an efficiency of 96.41 %, an improvement of 2 ms is observed in the starting characteristics. The above concept has been extended to single phase AC photovoltaic system with improvement of 15 % in its performance. It has benefits of high efficiency and low harmonic distortion at output voltage waveform. Here DC-DC boost converter and space vector modulation based inverter are used to provide the required supply to the load. The proposed T2NF based MPPT improves the system efficiency even at abnormal weather conditions. Here a lot of reduction in torque and current ripple contents is obtained with the help of T2NF based MPPT for an asynchronous motor drive. Also the better performance of an asynchronous motor drive is analyzed with the comparison of conventional and proposed MPPT controller using Matlab-simulation results. Practical validations are also carried out and tabulated.

**Keywords:** Photovoltaic (PV) system, Maximum power point tracking (MPPT) controller, Type 2 neuro fuzzy (T2NF) system, DC-DC boost converter, Space vector modulation (SVM), Abnormal weather conditions, Asynchronous motor (ASM) drive and harmonic distortion.

## 1. Introduction

The PV power and voltage characteristics are nonlinear and affected by the irradiance and temperature variations. The applied MPPT uses a type of control and logic to look for the knee, which in turn allows the converter to extract the maximum power from the PV array. The tracking method provides a new reference signal for the controller and extracts the maximum power from the PV array. The hill climbing method has slow response especially under varying weather conditions because the MPPT gives the decision directly for the duty cycle declaring a controller of error signal [1-3]. The voltage based MPPT method uses the fact that the ratio between the maximum power voltage and the open circuit voltage under different weather conditions, which are linearly proportional [4]. Perturbation and observation method are commonly used due to its ease of implementation, also works effectively under varying weather

conditions where it can reach to the error signal due to its separation between the MPPT method that controls the reference signal and duty cycle resulting of changing the reference signal [5-6].

Among different intelligent controllers, fuzzy logic is the simplest to integrate with the systems. Recently, fuzzy logic controller has received an increasing attention to researchers for converter control, motor drives and other process control as it provides better responses than other conventional controllers [7]. The imprecision of the weather variations that can be reflected by PV arrays also addressed accurately using fuzzy controller. Here Type 2 fuzzy based technique is implemented for PV system which is involved in the operation of fuzzification, inference and output processing. This output processing consists of type reduction and defuzzification to provide the better performance. The T2FLC deals with the variable step size to increase or decrease the reference voltage. Therefore the tracking time becomes short and the system performance during steady state conditions is much better than other conventional techniques [8-10].

Intelligent controls using artificial intelligence, fuzzy logic and neural networks, these systems are introduced as major sources to improve the performance of motor drives. Intelligent controls with adaptive network techniques are creating an interest research for practical implementation and control of motor drives. Earlier sinusoidal pulse width modulation (SPWM) was majorly used technique for industrial applications, because it reduces the harmonics. SPWM is suitable up to 0.7855 modulation indices for linear modulation index and above it gives more ripples in voltage [11-13]. To overcome this third harmonic injected pulse width modulation SVPWM techniques are used to improve the total harmonic distortion in voltage and current. Also it increases the modulation index up to 0.907 with increasing the fundamental value compared to SPWM [14-16]. Here the speed of the induction motor can also be controlled by direct torque control with PIC. But it cannot give good transient and steady state responses [17]. To overcome this, a new technique with type-2 fuzzy logic systems has been introduced as an upgrading of ordinary fuzzy logic set which is called type-1 fuzzy set. The characterization of type-2 fuzzy set is that the membership value for each element of this set is a fuzzy set in [0,1], not a crisp set like type-1 fuzzy. Type-2 fuzzy set can handle linguistics as well as numerical uncertainties. Because it can be modeled with reducing their effects [18-19].

Unfortunately, type-2 fuzzy sets are more difficult to use and understand than traditional type-1 fuzzy sets. Though it has few difficulties, it being used for many applications like coded video streams, co-channel interference elimination from nonlinear time-varying communication channels, connection admission control, extracting knowledge from questionnaire surveys, forecasting of time-series, function approximation, pre-processing radiographic images and transport scheduling with some control applications [20-21]. A comparison of adaptive neuro fuzzy based space vector modulation with neural network and conventional based system has been presented [22-23]. Here type-2 neuro fuzzy logic controller based MPPT method is proposed with boost converter to regulate the PV output voltage and track the MPP of PV modules and also to determine the system operation point which varies with load, solar irradiation and temperature variations.

So this paper proposes a novel type 2 neuro fuzzy based MPPT controller which takes variable irradiance and variable temperature into the consideration in order to get performance better than the existed methods. The advantage of this proposed MPPT algorithm is used to control the MPP even under abnormal weather conditions compared to other conventional algorithms. In section 2 mathematical modeling of PV array is discussed. Section 3 & 4 explains about the type 2 neuro fuzzy system and a novel type 2 neuro fuzzy based MPPT controller. Mathematical modeling of asynchronous motor drive is noted in section 5. Section 6 states a brief note on proposed space vector modulation technique. Using the proposed MPPT along with DC-DC converter to boost up the PV output and to feed asynchronous motor drive is detected in section 7. Matlab-simulation results with the comparison of conventional and proposed MPPT techniques are presented in section 8. The concluding remarks are stated in section 9.

## 2. Mathematical Modeling of PV Array

Solar PV system is made of photovoltaic cells. Cells are grouped to form panels and panels are grouped to form array. The basic mathematical equations describes the ideal PV cell and those are clearly mentioned in equations (1) and (2)

$$I_M = I_{PVCELL} - I_{OCELL}\left[\frac{\exp\left(\frac{QV_M}{KNT_{AP}}\right)}{I_d} - 1\right], \quad (1)$$

where $I_{PVCELL}$ is the incident light generated current, $I_{OCELL}$ is the diode reverse saturation current, Q is the charge of an electron at $1.602\times10^{-19}$ C, K is the Boltzmann's constant at $1.381\times10^{-23}$ J/K, $T_{AP}$ is the temperature at the junction in Kelvin, N is the diode identity constant, $V_{PVCELL}$ is the voltage across the PV cell and $I_{PVCELL}$ is the current of the ideal PV model as illustrated in Fig. 1.

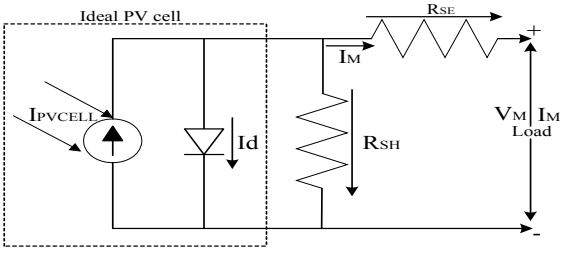


**Fig. 1.** Practical PV cell equivalent circuit.

PV system basic equation does not represent I-V characteristics, as a practical PV module consists of various PV cells which require additional parametric values as series and parallel resistances ($R_{SE}$ & $R_{SH}$) as shown in Fig. 1. PV module modeling is based on mathematical equation of the solar cell which is given by Eq. 2.

$$I_M = I_{PVCELL} - I_{OCELL}\left[exp^{\frac{Q(V_M+I_MR_{SE})}{N_TKNT_{AP}}} - 1\right] - \frac{V_M+I_MR_{SE}}{R_{SH}} \quad (2)$$

where $I_M$ = PV module current in Amps, $I_{PVCELL}$ = Photocurrent or light generated current in Amps, $I_{OCELL}$ = Reverse saturation current of a diode in Amps, $Q$ = Electron charge in Coulombs, $N$ = Ideality factor (taken from data sheet), $K$ = Boltzmann constant in J/°K, $T_{AP}$ = Applied temperature for the PV module in Kelvin, $V_M$ = Module voltage in Volts, $R_{SE}$ = Series resistance in ohms, $R_{SH}$ = Parallel resistance in ohms and Current generated by light ($I_{PVCELL}$) depends linearly on solar radiation and also on temperature is given by Eq. (3)

$$I_{PVCELL} = \frac{P_{AP}[I_{SCR}+T_{SCI}(T_{AP}-T_{REF})]}{P_{REF}} \quad (3)$$

where $P_{AP}$ = Applied solar irradiance in W/m$^2$ (applied to the module during the experiment), $P_{REF}$ = Reference irradiance in W/m$^2$ (1000 W/m$^2$ is taken under STC), $I_{SCR}$ = Module short circuit current (taken from the data sheet), $T_{SCI}$ = Temperature coefficient of short circuit current in A/°K (taken from data sheet), $T_{AP}$ and $T_{REF}$ are applied and reference temperatures in Kelvin. The practical calculated $I_{PV\ CELL}$ values for different irradiance and different temperature are tabulated in Table. 1.

**Table 1.** The Practical Calculated $I_{pv\ Cell}$ Values for Different Irradiance and Different Temperature.

| Irradiance in (W/m$^2$) | Temperature (in °C) | | | | |
|---|---|---|---|---|---|
| | ***20 °C*** | ***30 °C*** | ***40 °C*** | ***50 °C*** | ***60 °C*** |
| 1000 | 8.661 | 8.678 | 8.695 | 8.712 | 8.729 |
| 800 | 6.929 | 6.942 | 6.956 | 6.97 | 6.983 |
| 500 | 4.330 | 4.339 | 4.347 | 4.356 | 4.364 |
| 250 | 2.165 | 2.169 | 2.173 | 2.178 | 2.182 |
| 100 | 0.866 | 0.867 | 0.869 | 0.871 | 0.872 |
| 50 | 0.433 | 0.433 | 0.434 | 0.435 | 0.436 |
| 10 | 0.086 | 0.086 | 0.086 | 0.087 | 0.087 |

Modules reverse saturation current ($I_{RS}$) at nominal condition and reference temperature is given by Eq. (4)

$$I_{RS} = \frac{I_{SCR}}{exp^{\left(\frac{QV_{OC}}{N_TKNT_{AP}}\right)}-1} \quad (4)$$

where $I_{RS}$ = Reverse saturation current in Amps, and $N_T$ = total no. of cells in a module. Here module voltage decreases as the applied temperature goes on increases which can be calculated by Eq. (5)

$$V_M = \frac{N_TKNT_{AP}}{Q} \times \ln\left[\frac{I_{PVCELL}-I_{RS}}{I_{RS}}\right] \quad (5)$$

On the other hand saturation current ($I_{SAT}$) is given as

$$I_{SAT} = I_{RS} \times \left(\frac{T_{AP}}{T_{REF}}\right)^3 \times exp^{\left\{\frac{QE_{GO}}{NK}\left(\frac{1}{T_{REF}}-\frac{1}{T_{AP}}\right)\right\}} \quad (6)$$

where $E_{GO}$ = is the semiconductor band gap energy of the module in J/C. The resistance $R_{SH}$ is inversely proportional to leakage current and a small variation of series resistance will affect the PV output power. A PV cell will produce less than 2 watts at approximately 0.5 V. The cells must be connected in series and parallel to get required power. Array basic output current of single diode module is calculated by Eq. (7)

$$I_A = N_{PV}\, I_{PVCELL} - N_{PR}I_{OCELL}\left[exp^{\frac{Q}{N_TKNT_{AP}}\left(\frac{V_M}{N_{SE}}+\frac{I_MR_{SE}}{N_{PR}}\right)} - 1\right] - \frac{1}{R_{SH}}\left[\frac{N_{PR}V_M}{N_{SE}} + I_MR_{SE}\right] \quad (7)$$

where $N_{SE}$ and $N_{PR}$ are the number of solar cells connected in series ad parallel. Modeling of PV array is done based on data sheet parameters of SSI-3M6-250W poly-crystalline solar module at 25° C and 1000 W/m$^2$. Based on above parameters PV is modeled in Simulink model is developed under standard test conditions.

## 3. Type-2 Neuro Fuzzy Controller

In this section, the structure and mechanism of T2NFIS is presented. The structure of T2NFIS is shown in Fig. 2. It is a five layered network which uses type-2 neuro fuzzy sets in the antecedent and the consequent realizes the Takagi-Sugeno-Kang Type-0 fuzzy inference mechanism. Let assume the structure consists of q input features, n output features and has grown K rules after processing t-1 samples. Hereafter, we detail the function of each layer when the network is presented with the t$^{th}$ sample, x(t).

**Layer 1 - Input layer**

Each node in this layer passes the input data directly to the fuzzification layer. The output of i$^{th}$ node is given as in Eq. (8) and the diagram is shown in Fig. 2.

$$u_i(t) = x_i(t), \text{ where } i = 1, 2, \cdots, q \quad (8)$$

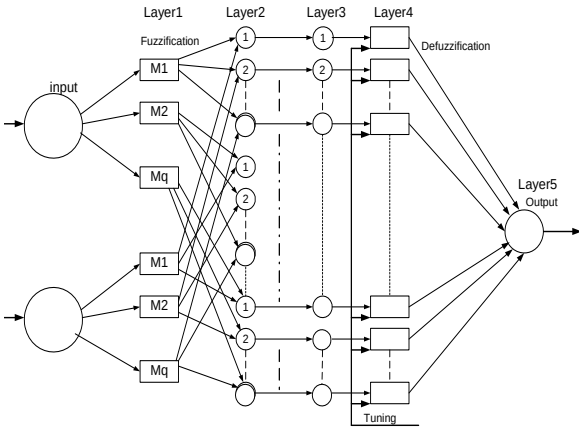


**Fig. 2.** Structure of five layered type-2 neuro-fuzzy system.

**Layer 2 - Fuzzification layer**

The function of this layer is to perform the fuzzification operation. Each node in this layer computes the Type-2 membership of the input with the rule antecedents. The membership of i[th] input feature with k[th] rule is given by:

$$\emptyset_{ki}(t) = exp^{(-\frac{(u_i(t)-\mu_{ki})^2}{2\sigma_{ki}^2} \equiv \emptyset(\mu_{ki},\sigma_{ki},u_i(t))} \quad (9)$$

where $\mu_{ki} \in [\mu_{ki}^l, \mu_{ki}^r]$ and $\sigma_{ki} \in [\sigma_{ki}^l, \sigma_{ki}^r]$. Are left and right limits of the center and width of k[th] rule's i[th] feature respectively. The footprint of uncertainty of this membership function can be represented in terms of upper membership function $\varphi_{up}$ and lower membership function $\varphi_{lo}$ as given below

$$\emptyset_{ki}^{up}(t) = \{ \begin{matrix} \emptyset\left(\mu_{ki}^l,\sigma_{ki}^l,u_i(t)\right) \\ \emptyset\left(\mu_{ki}^r,\sigma_{ki}^r,u_i(t)\right) \end{matrix} \quad (10)$$

where $u_i(t) < \mu_{ki}^l, \mu_{ki}^l \le u_i(t) \le \mu_{ki}^r, u_i(t) > \mu_{ki}^r$

$$\emptyset_{ki}^{lo} = \{ \begin{matrix} \emptyset\left(\mu_{ki}^r,\sigma_{ki}^r,u_i(t)\right) u_i(t) \le \frac{\mu_{ki}^l + \mu_{ki}^r}{2} \\ \emptyset\left(\mu_{ki}^l,\sigma_{ki}^l,u_i(t)\right) u_i(t) > \frac{\mu_{ki}^l + \mu_{ki}^r}{2} \end{matrix} \quad (11)$$

The output of each node can be represented as

$$\emptyset_{ki} = [\emptyset_{ki}^{lo}(t), \emptyset_{ki}^{up}(t)] \quad (12)$$

**Layer 3 - Firing layer**

The firing layer consists of K nodes where each node represents the upper and lower antecedent part of a fuzzy rule. The function of this layer is to calculate the firing strength of each of the rules. The algebraic product operation is used to compute the firing strength of a rule and is given by

$$[F_k^{lo}(t), F_k^{up}(t)]; k = 1, \dots, K \quad (13)$$

$$[F_k^{lo}(t) = \prod_{i=1}^{m} \emptyset_{ik}^{lo} \; and \; F_k^{up}(t) = \prod_{i=1}^{m} \emptyset_{ik}^{up} ;$$

$$k = 1, \dots, K \quad (14)$$

**Layer 4 - Interval-reduction layer**

This layer contains K nodes. The function of each node is to perform the interval- reduction of Interval Type-1 fuzzy set to Type-1 fuzzy number. The computationally efficient algorithm is employed to reduce the interval and is given as

$$F_k(t) = \propto F_k^{lo}(t) + (1-\propto)F_k^{up}(t); k = 1, \dots \dots, K \quad (15)$$

where α is the design vector. In our study α is chosen as 0.5.

**Layer 5- Output layer**

This layer computes the output of network by employing weighted average defuzzification technique and is given as

$$\hat{Y}_j(t) = \frac{\sum_{k=1}^{K} w_{jk} F_k(t)}{\sum_{p=1}^{K} F_p(t)}; j = 1, \dots, n \quad (16)$$

where $w_{jk}$ is the output weight connecting the k[th] rule with the j[th] output node.

## 4. Novel Type-2 Neuro Fuzzy based MPPT Controller

TIFLCs are unable to handle rule uncertainties directly, because they will not use type-2 neuro fuzzy (T2NF) sets that are certain. On the other hand T2NFLC is very useful in uncertainties measurement with minimizing the effects of uncertainties in rule base. Because their use is not widespread yet. In this one should identify the main control variables and determine the sets that describe the values of each linguistic variable. This algorithm is designed to achieve the advantage of other MPPT algorithms to simplify and eliminate all aforementioned drawbacks. The change in PV array output and the change in PV array output voltage are the inputs of the T2NF. The increment of the reference voltage is the output of the T2NFLC where the increment is added to the previous reference voltage to produce the new reference voltage. The inputs and the outputs of the T2NFLC are shown in the equations from (17) to (19)

$$\Delta P = P(k) - P(k-1) \quad (17)$$

$$\Delta V = V(k) - V(k-1) \quad (18)$$

$$\Delta Vref = Vref(k) - Vref(k-1) \quad (19)$$

The differential power dp can be calculated as

$$dP = Pmax - Pmin \quad (20)$$

Flow chart of type-2 neuro fuzzy based MPPT algorithm is shown in Fig. 3.

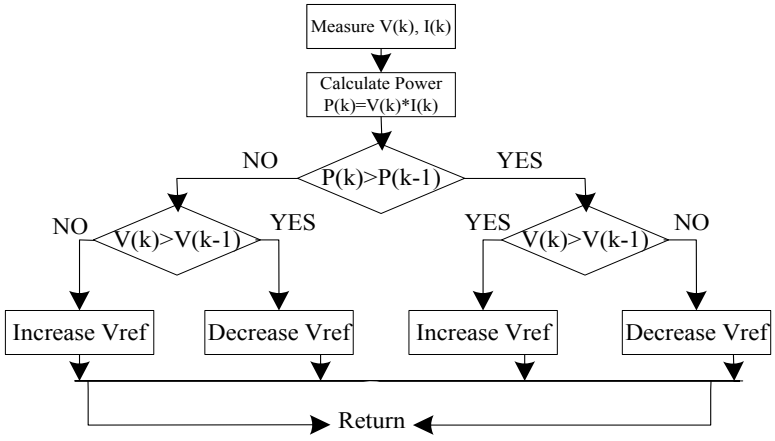


**Fig. 3.** Flowchart of type-2 neuro fuzzy based MPPT algorithm for power improvement.

The input variables of the T2NFLC are divided into 4 subsets as positive big (PB), positive small (PS), negative small (NS), negative big (NB). Also, the membership functions of the output variables are four fuzzy sets, where the maximum of minimum composition technique is used for the inference and the gravity method for defuzzification process to convert the fuzzy subset reference voltage changes to real members as presented in (21)

$$\Delta Vref = \frac{\sum_i^n \Delta Vrefi\ \mu(\Delta Vrefi)}{\sum_i^n \mu(\Delta Vrefi)} \quad (21)$$

where $\Delta Vref$ is the fuzzy output and $\Delta Vrefi$ is the output membership functions of max-min interference composition. $\Delta Vref$ is the increasing function with respect Vref. The left most point VrefL and right most point VrefR can be obtained as follows

$$\Delta VrefL = \frac{\sum_i^n \Delta VrefLi\ \mu(\Delta VrefLi)}{\sum_i^n \mu(\Delta VrefLi)} \quad (22)$$

$$\Delta VrefR = \frac{\sum_i^n \Delta VrefRi\ \mu(\Delta VrefRi)}{\sum_i^n \mu(\Delta VrefRi)} \quad (23)$$

The defuzzified crisp output from the type-2 fuzzy system is the average of VrefL and VrefR as

$$\Delta Vref = \frac{\Delta VrefR + \Delta VrefL}{2} \quad (24)$$

But from equations (17), (18) and (20) Pmax and Pmin we get as follows

$$Pmax = Vpv\_(k-1) * Ipv\_(k-1) \quad (25)$$

$$Pmin = Vpv\_k * Ipv\_k \quad (26)$$

This algorithm modifies the phase displacement between grid voltage and the converter voltage providing the voltage reference Vref. Furthermore, here an extra feature is added to monitor the maximum and minimum power oscillations on the PV side. In case of single-phase power systems, the instant power oscillates with the line frequency. If the system operates in the area around MPP, the ripple of the power on the PV side is minimized. A flow chart of the MPPT explains how the angle of the reference voltage is modified in order to keep the operating point as close to MPP.

The phase displacement d$\delta mppt$ is provided by the controller. If that the operating in the area on the left side of the MPP then d$\delta mppt$ has to decrease. This decrement is indicated with side=-1. Moreover, if the operating in the area on the right side of the MPP then d$\delta mppt$ has to increase and it is indicated with side =+1. The increment size determines how fast the MPP is tracked. The measure of the power oscillations on the PV side is used to quantify the increment that is denoted.

## 5. Mathematical Modeling of Asynchronous Motor Drive

The mathematical modeling of a three-phase, squirrel-cage asynchronous motor drive can be described with stationary reference frame as

$$V_{qS} = (R_S + pL_S)I_{qS} + PL_M I_{qR} \quad (27)$$

$$V_{dS} = (R_S + pL_S)I_{dS} + PL_M I_{dR} \quad (28)$$

$$0 = pL_M I_{qS} - \omega_R L_M I_{dS} + (R_R + pL_R)i_{qR} - \omega_R L_R i_{dR} \quad (29)$$

$$0 = \omega_R L_M i_{qS} + pL_M i_{dS} + \omega_R L_R i_{qR} + (R_R + pL_R)i_{dR}, \quad (30)$$

where $\omega_R = \frac{d\theta}{dt}$, $p = \frac{d}{dt}$

Suffixes S and R represents stator and rotor respectively. $V_{dS}$ and $V_{qS}$ are d-q axis stator voltages respectively, $i_{dS}$, $i_{qS}$ and $i_{dR}$, $i_{qR}$ are d-q axis stator currents and rotor currents respectively. $R_S$ and $R_R$ are stator and rotor resistances per phase. $L_S$, $L_R$ are self inductances of stator and rotor and $L_M$ is mutual inductance. Stator and rotor flux linkages can be expressed as

$$\lambda_{qS} = L_S i_{qS} + L_M i_{qR} \quad (31)$$
$$\lambda_{dS} = L_S i_{dS} + L_M i_{dR} \quad (32)$$
$$\lambda_{qR} = L_R i_{qR} + L_M i_{qS} \quad (33)$$
$$\lambda_{dR} = L_R i_{dR} + L_M i_{dS} \quad (34)$$

From the above equations (27)-(30), Squirrel-cage asynchronous motor can described by following equations in stator reference frame as

$$\begin{bmatrix} V_{qS} \\ V_{dS} \\ 0 \\ 0 \end{bmatrix} = \begin{bmatrix} R_S + pL_S & 0 & pL_M & 0 \\ 0 & R_S + pL_S & 0 & pL_M \\ pL_M & -\omega_R L_R & R_R + pL_R & -\omega_R L_R \\ \omega_R L_M & pL_M & \omega_R L_R & R_R + pL_R \end{bmatrix} \begin{bmatrix} i_{qS} \\ i_{dS} \\ i_{qR} \\ i_{dR} \end{bmatrix} \quad (35)$$

The electromagnetic torque Te of the induction motor is given by

$$T_e = \frac{3}{2}\left(\frac{p}{2}\right)\left(\lambda_{qR} i_{dR} - \lambda_{dR} i_{qR}\right) \quad (36)$$

From the dynamic model of asynchronous machine, the rotor flux is aligned along with the d-axis then the q-axis rotor flux $\lambda_{qR}$=0. So from the equations (33 and 36) described in the previous section and putting $\lambda_{qR}$=0, the electromagnetic torque of the motor in the vector control can be expressed as

$$T_e = \frac{3}{2}\left(\frac{p}{2}\right)\frac{L_M}{L_R}\left(\lambda_{dR} i_{qS}\right) \quad (37)$$

If the rotor flux linkage $\lambda_{dR}$ is not disturbed, the torque can be independently controlled by adjusting the stator q- component current $i_{qS}$. As the rotor flux aligned on d-axis, this leads to $\lambda_{qR}$=0 and $\lambda_{dR}$=$\lambda_R$, then

$$\omega_{sl} = \frac{L_M R_R}{\lambda_R L_R} i_{qS} \quad (38)$$

## 6. Proposed SVM Technique for Two-Level Inverter

In this the space vector modulation algorithm for two level inverter is introduced for which the solar panels are connected to provide the dc supply. SVM basic principle and switching sequence is given in order to get symmetrical algorithm pulses and voltage balancing. This scheme is used to control the output voltage of the two level inverter with the T2NF based MPPT controller. In the SVM algorithm, the d-axis and q-axis voltages are converted into three-phase instantaneous reference voltages. Then the imaginary switching time periods proportional to the instantaneous values of the reference phase voltages. Which are defined as

$$T_{U1} = \left(\frac{T_S}{V_{DC}}\right) V_{U1}^*, T_{V1} = \left(\frac{T_S}{V_{DC}}\right) V_{V1}^*, T_{W1} = \left(\frac{T_S}{V_{DC}}\right) V_{W1}^* \quad (39)$$

where $T_S$ and $V_{DS}$ are the sampling interval time and dc link voltage respectively. Here the sampling frequency is the twice the carrier frequency.

Then the maximum (MAXI), middle (MID) and minimum (MINI) imaginary switching times can be in each sampling interval by using (40)-(42)

$$T_{MAXI} = MAXI(T_{U1}, T_{V1}, T_{W1}) \quad (40)$$
$$T_{MINI} = MINI(T_{U1}, T_{V1}, T_{W1}) \quad (41)$$
$$T_{MID} = MID(T_{U1}, T_{V1}, T_{W1}) \quad (42)$$

The active voltage vector switching times $T_1$ and $T_2$ are calculated as

$$T_1 = T_{MAXI} - T_{MID} \text{ and } T_2 = T_{MID} - T_{MINI} \quad (43)$$

The zero voltage vectors switching time is calculated as

$$T_Z = T_s - T_1 - T_2 \quad (44)$$

The zero state time will be shared between two zero states as $T_0$ for $V_0$ and $T_7$ for $V_7$ respectively, and can be expressed as

$$T_0 = K_0 T_Z \quad (45)$$
$$T_7 = (1 - K_0) T_Z \quad (46)$$

Here $K_0$ is taken as 0.5 to obtain the SVM algorithm. The various SVM algorithms can be generated by changing $K_0$ between zero and one. However, in this SVM algorithm, the zero voltage vector time distributed equally among $V_0$ and $V_7$ as shown in Fig. 4.

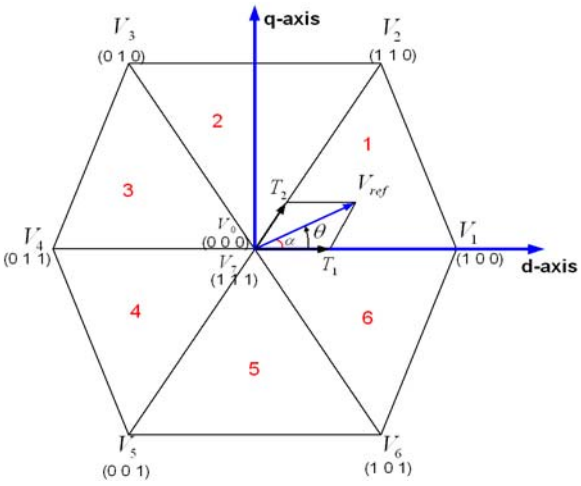


**Fig. 4.** Space vector diagram.

## 7. Proposed MPPT System with DC-DC Converter, Inverter and ASM Drive

The below system represents the proposed system structure with DC-DC converter. In this, PV array contains 6 PV modules with 250 Watts each; these modules are connected in series and parallel to yield better output voltage and current. The proposed type 2 neuro fuzzy (T2NF) based MPPT algorithm extracts the maximum power from solar PV array.

The point of operation of the PV array is adjusted by varying the duty cycle. DC-DC converter boosts the PV array voltage and also increases the maximum utilization of PV array by operating at MPP. Boost converter increases the array output voltage up to 400 Volts with the help of SVM based inverter. The minimum inductor value ($L_{MIN}$) is calculated from Eq. (47) to ensure the continuous inductor current.

$$L_{MIN} = \left(\frac{V_0(1-D)^2 \times D}{2}\right) \times f_S \times I_{AVG} \quad (47)$$

where $V_0$ is the DC output voltage, D is the duty ratio, $f_S$ is the switching frequency of the converter, $I_{AVG}$ is the average output current. The minimum capacitance value ($C_{MIN}$) can be calculated using Eq. (48)

$$C_{MIN} = \frac{V_0 \times D}{R \times \Delta V_0 \times f_S} \quad (48)$$

The switching frequency selection is trade-off between switching losses, cost of switch and the converter efficiency.

## 8. Results and Discussion

Simulation results are obtained under different operating conditions taking the reference value of speed as 1200 rpm. The results obtained with conventional MPPT and proposed type 2 neuro fuzzy (T2NF) based MPPT controller are given in Fig. 5-22.

### 8.1. Simulation Results of Asynchronous Motor Drive at starting

For the asynchronous motor drive the maximum current and the ripple content in the torque is reduced during starting in order to reach the early steady state. With the proposed type 2 neuro fuzzy (T2NF) based MPPT the maximum torque, stator phase current and the speed are obtained as 12.5 N-m, 20 Amps and 1200 RPM respectively. It is observed that the ripple content in the torque is reduced a lot compared to the other existed methods. Due to this better speed response is obtained. These results are presented in Figs. 5-7.

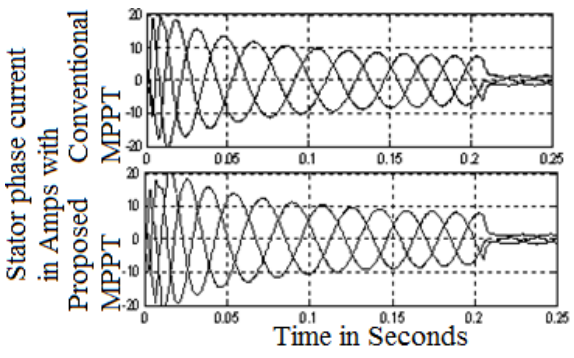


**Fig. 5.** Stator phase current responses with conventional and proposed T2NF based MPPT controller during starting.

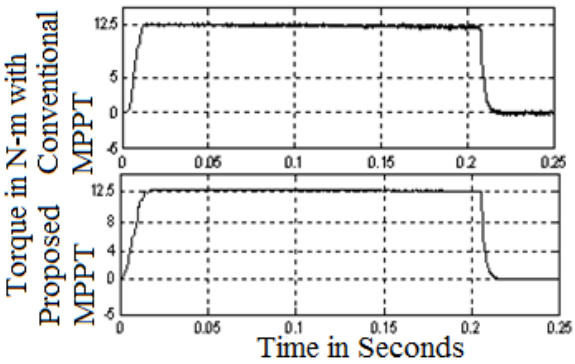


**Fig. 6.** Torque responses with conventional and proposed T2NF based MPPT controller during starting.

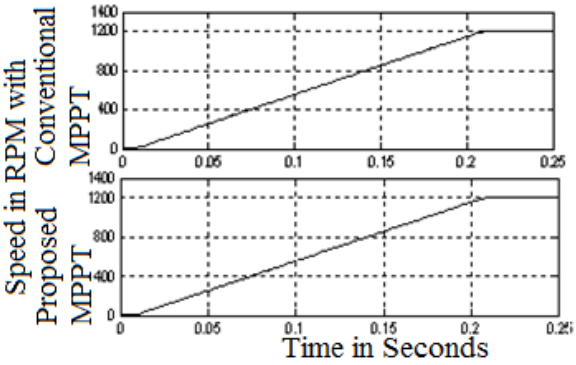


**Fig. 7.** Speed responses with conventional and proposed T2NF based MPPT controller during starting.

### 8.2. Simulation Results of Asynchronous Motor Drive at steady state condition

Here torque ripple with the proposed MPPT is reduced i.e. it is observed that the torque ripple with the conventional and proposed MPPT are 0.48 and 0.09 respectively. The better speed response is obtained with the proposed T2NF based MPPT controller. The steady state responses of the stator phase currents, torque and speed with conventional and proposed MPPT are observed in Figs. 8-10.

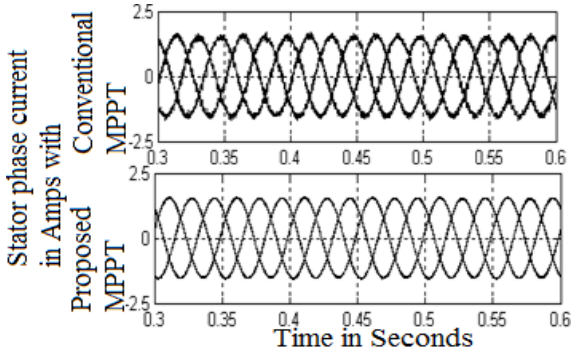


**Fig. 8.** Stator phase current responses with conventional and proposed T2NF based MPPT controller during steady state.

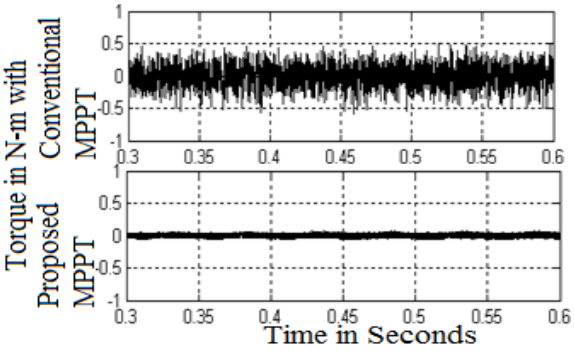


**Fig. 9.** Torque responses with conventional and proposed T2NF based MPPT controller during steady state.

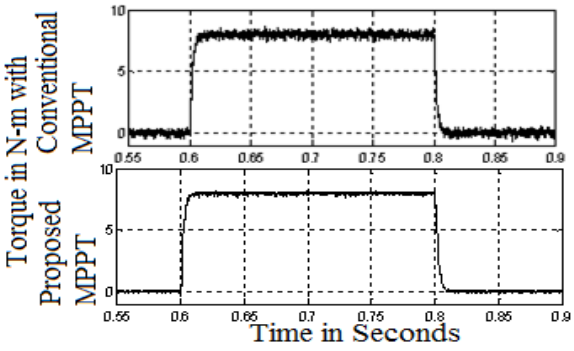


**Fig. 12.** Torque responses with conventional and proposed T2NF based MPPT controller during step change in load.

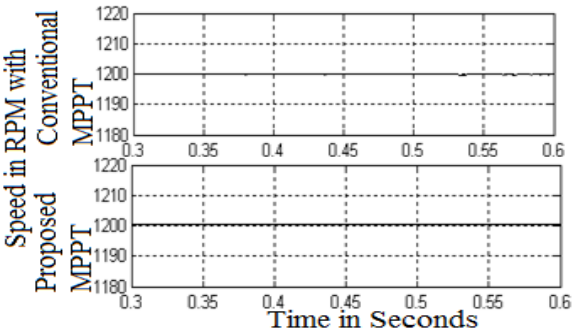


**Fig. 10.** Speed responses with conventional and proposed T2NF based MPPT controller during steady state.

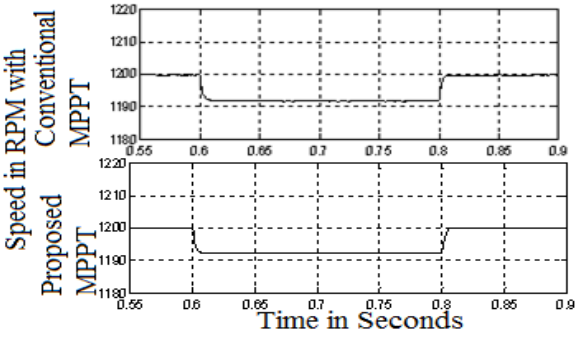


**Fig. 13.** Speed responses with conventional and proposed T2NF based MPPT controller during step change in load.

### 8.3. Simulation Results of Asynchronous Motor Drive at transients with step change in load

The ripple content in the current and torque is reduced with the proposed T2NF based MPPT. Also the speed decrement is little less with the proposed T2NF based MPPT during the load change. The response during the transients with step change in load torque of 8 N-m is applied at 0.6 sec and removed at 0.8 sec is shown in Figs. 11-13.

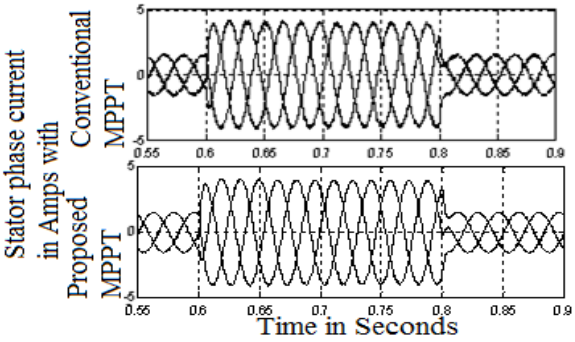


**Fig. 11.** Stator phase current responses with conventional and proposed T2NF based MPPT controller during step change in load.

### 8.4. Simulation Results of Asynchronous Motor Drive at transients with the speed reversal operation from +1200 to -1200 RPM

The overall performance of the drive is improved with the proposed T2NF MPPT controller and the speed response reaches the reference value earlier compared to other existed methods. The results of the drive during speed reversals from +1200 to -1200 RPM are observed in Figs. 14-16.

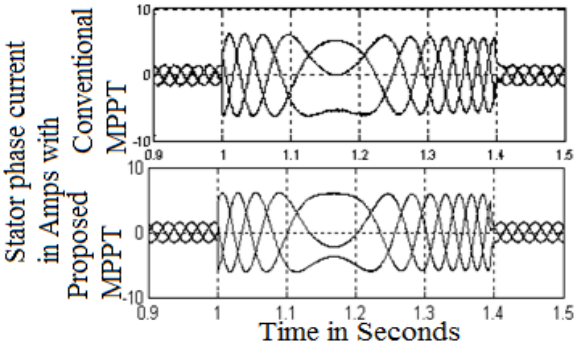


**Fig. 14.** Current responses with conventional and proposed T2NF based MPPT controller during transients at speed reversal from +1200 to -1200 RPM.

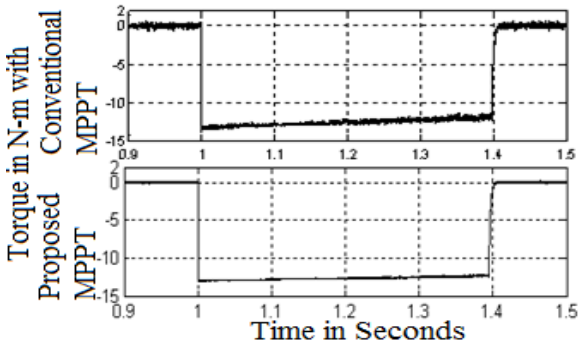


**Fig. 15.** Torque responses with conventional and proposed T2NF based MPPT controller during transients at speed reversal from +1200 to -1200 RPM.

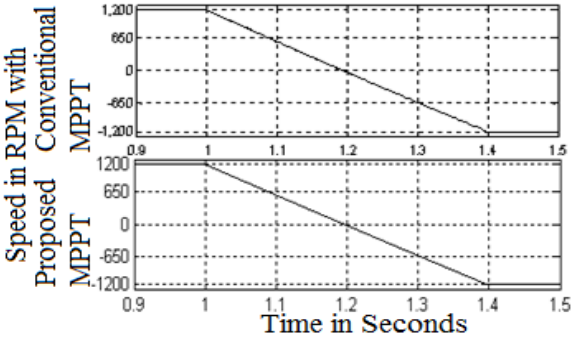


**Fig. 16.** Speed responses with conventional and proposed T2NF based MPPT controller during transients at speed reversal from +1200 to -1200 RPM.

### 8.5. Simulation Results of Asynchronous Motor Drive at transients with the speed reversal operation from -1200 to +1200 RPM

The overall performance of the drive is improved with the proposed T2NF based MPPT controller and the speed response reaches the little earlier compared to conventional methods. The results of the drive during speed reversals from -1200 to +1200 RPM are observed in Figs. 17-19.

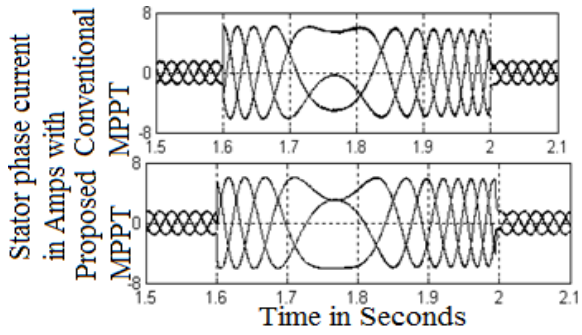


**Fig. 17.** Current responses with conventional and proposed T2NF based MPPT controller during transients at speed reversal from -1200 to +1200 RPM.

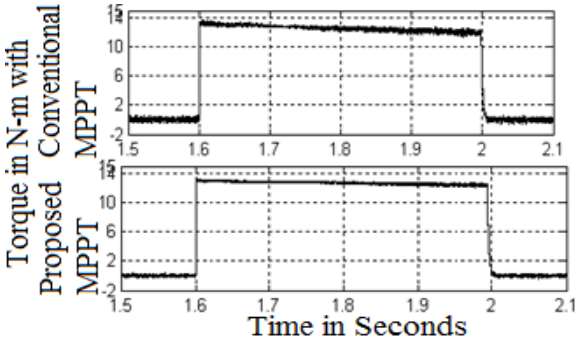


**Fig. 18.** Torque responses with conventional and proposed T2NF based MPPT controller during transients at speed reversal from -1200 to +1200 RPM.

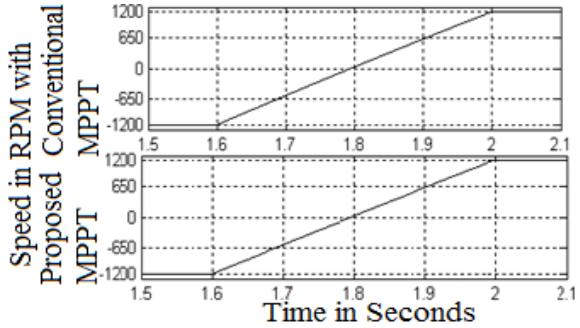


**Fig. 19.** Spedd responses with conventional and proposed T2NF based MPPT controller during transients at speed reversal from -1200 to +1200 RPM.

## 9. Conclusion

The PV array model with the type 2 neuro fuzzy (T2NF) based MPPT controller is tested. From this the performance of the asynchronous motor drive is analyzed with comparing the both conventional and proposed type 2 neuro fuzzy based MPPT controller results. Also the behavior of the proposed T2NF MPPT is observed with practical validations during a partially cloudy day. PV system with DC-DC boost converter and space vector modulation based technique inverter enhances the system performance even under abnormal weather conditions. The ripple contents in the torque and stator phase currents are reduced a lot with the proposed T2NF based MPPT controller. Here the early steady state response of the motor drive is reached along with attaining of better speed response. Thus the utilization and efficiency of the system is improved much with the proposed T2NF based MPPT controller.

## Acknowledgement

The funding support given by SERB, Department of Science and Technology (DST), Government of India with No. SERB/ET-069/2013 for the solar based project is acknowledged.

## References


[1]. O. Uncu and I. Turksen, Discrete interval type-2 fuzzy system models using unvertainty in learning raramenters, *IEEE Trans, Fuzzy Systems*, Vol. 15, No. 1, 2007, pp. 90-106.

[2]. L. Fangrui, D. Shanxu, L. Fei, L. Bangyin, and K. Yong, A variable step size INC MPPT method for PV systems, *IEEE Trans, Industrial Electronics*, Vol. 55, No. 7, 2008, pp. 2622–2628.

[3]. B. Pakkiraiah and G. Durga Sukumar, Research Survey on Various MPPT Performance Issues to Improve the Solar PV System Efficiency, *Journal of Solar Energy,* Vol. 2016, No. 2016, 2016, Article ID 8012432, pp. 1-20.

[4]. M. A. Masoum, H. Dehbonei, and E. F. Funchs, Theoretical and experimental analyses of photovoltaic systems with voltage and current-based maximum power point tracking, *Power Eng. Rev., IEEE*, Vol. 22, No. 8, 2002, pp. 62–62.

[5]. N. Femia, G. Petrone, G. Spagnuolo, and M. Vitelli, Optimizing duty cycle perturbation of P&O MPPT technique, in *Proceedings of the IEEE 35th Annu. Power Electron. Spec. Conf.,* Vol. 3, 2004, pp. 1939–1944.

[6]. B. Pakkiraiah and G. Durga Sukumar, A New Modified MPPT Controller for Solar Photovoltaic System, in *Proceedings of the IEEE International Conference on Research in Computational Intelligence and Communication Networks (ICRCICN)*, 2015, pp. 294-299.

[7]. M. F. Naguib and L. A. C. Lopes, Harmonics reduction in current source converter using fuzzy logic, *IEEE Transactions on Power Electronics*, Vol. 25, No. 1, 2010, pp. 158-167.

[8]. M. M. Rashid, N. A. Rahim, M. A. Hussain and M. A. Rahman, Analysis and experimental study of magnetorhological based damper for semiactive suspension system using fuzzy hybrids, *IEEE Transcations on Industrial Applications*, Vol. 47, No. 2, 2011, pp. 1051-1059.

[9]. M. Singh and A. Chandra, Appilcation of adaptive network- based fuzzy interface system for sensorless control of PMSG-based wind turbine with non linear load compensation capabilities, *IEEE Transactions on Power Electronics*, Vol. 26, No. 1, 2011, pp. 165-175.

[10]. B. N. Alajmi, K. H. Ahmed, S. J. Finney and B. W. Williams, Fuzzy-logic-control approach of a modified hill-climbing method for maximum power point in microgrid standalone system, *IEEE Transactions on Power Electronics*, Vol. 26, No. 4, 2011, pp. 1022-1030.

[11]. Alexis Kwasinski, Philip T. Krein, and Patrick L. Chapman, Time Domain Comparison of Pulse-Width Modulation Schemes, *IEEE Trans on Power Electronics*, Vol. 1, No. 3, 2003, pp. 64-68.

[12]. G. Narayanan, Di Zhao, Harish and K. Krishnamurthy, Space Vector Based Hybrid PWM Techniques for Reduced Current Ripple*, IEEE Trans. on Ind. Electron*, Vol. 55, No. 4, 2008, pp. 1614-1627.

[13]. I. Takahashi and T. Noguchi, A new quick-response and high- efficiency control strategy of an induction motor, *IEEE Trans. Ind. Appl.,* Vol. 22, No. 5, 1986, pp. 820–827.

[14]. Bimal K. Bose, Power Electronics and Motor Drives Advances and Trends, *Academic Press is an Imprint of Elsevier*, 2006.

[15]. B. Pakkiraiah and G. Durga Sukumar, A New Modified MPPT Controller for Improved Performance of an Asynchronous Motor Drive under Variable Irradiance and Variable Temperature, *International Journal of Computers and Applications-Taylor & Francis*, 2016, pp. 1-14.

[16]. Peter Vas, Sensor less Vector and Direct Torque Control, *Oxford University Press*, 1998.

[17]. D. Casadei, G. Serra, A. Tani, L. Zarri and F. Profumo, Performance analysis of a speed-sensor less induction motor drive based on a constant switching-frequency DTC scheme, *IEEE Trans. Ind. Appl*., Vol. 39, No. 2, 2003, pp. 476–484.

[18]. N. N. Karnik, J. M. Mendel, and Q. Liang, Type-2 fuzzy logic systems, *IEEE Trans Fuzzy Systems*, Vol. 7, 1999, pp. 643-658.

[19]. J. M. Mendel and R. I. B. John, Type-2 fuzzy sets made simple, *IEEE Trans on Fuzzy System*, Vol. 10, 2002, pp. 117-127.

[20]. Q. Liang and J. M. Mendel, Interval type-2 fuzzy logic systems: Theory and design, *IEEE Trans on Fuzzy System*, Vol. 8, 2000, pp. 535 550.

[21]. Q. Liang, N. N. Karnik, and J. M. Mendel, Connection admission control in ATM networks using surveybased type-2 fuzzy logic systems, *IEEE Trans on Syst Man Cybern Part C*, Vol. 30, 2000, pp. 329-339.

[22]. Durga Sukumar, Jayachandranath Jitendranath and Suman Saranu, Three-level Inverter-fed Induction Motor Drive Performance Improvement with Neuro-fuzzy Space Vector Modulation, *Electrical Power Components and Systems-Taylor & Francis*, Vol. 42, No. 15, 2014, pp. 1633-1646.

[23]. B. Pakkiraiah and G. Durga Sukumar, A New Modified Adaptive Neuro Fuzzy Inference System Based MPPT Controller for the Enhanced Performance of an Asynchronous Motor Drive, in *Proceedings of the 1st International Conference on Advancement of Computer Communication & Electrical Technology (ACCET'16),* 21 – 22 October 2016.